RSC Advances

PAPER

View Article Online
View Journal | View Issue

Cite this: *RSC Adv.*, 2020, **10**, 19770

Synthesis, physicochemical characterization, toxicity and efficacy of a PEG conjugate and a hybrid PEG conjugate nanoparticle formulation of the antibiotic moxifloxacin†

Lesego L. Tshweu,[ab] Mohamed A. Shemis,[c] Aya Abdelghany,[c] Abdullah Gouda,[c] Lynne A. Pilcher,[b] Nicole R. S. Sibuyi,[d] Mervin Meyer,[d] Admire Dube[e] and Mohammed O. Balogun*[a]

Antibiotic resistance is increasing at such an alarming rate that it is now one of the greatest global health challenges. Undesirable toxic side-effects of the drugs lead to high rates of non-completion of treatment regimens which in turn leads to the development of drug resistance. We report on the development of delivery systems that enable antibiotics to be toxic against bacterial cells while sparing human cells. The broad-spectrum fluoroquinolone antibiotic moxifloxacin (Mox) was successfully conjugated to poly(ethylene glycol) (PEG) which was further encapsulated into the hydrophobic poly(ε-caprolactone) (PCL) nanoparticles (NPs) with high efficiency, average particle size of 241.8 ± 4 nm and negative zeta potential. Toxicity against erythrocytes and MDBK cell lines and drug release in human plasma were evaluated. Hemocompatibility and reduced cytotoxicity of the PEG–Mox and PCL(PEG–Mox) NPs were demonstrated in comparison to free Mox. Antimicrobial activity was assessed against drug sensitive and resistant: *Staphylococcus aureus*, *Escherichia coli*, *Pseudomonas aeruginosa* and *Klebsiella pneumoniae*. The antibacterial activity of Mox was largely maintained after conjugation. Our data shows that the toxicity of Mox can be effectively attenuated while, in the case of PEG–Mox, retaining significant antibacterial activity. At the conditions employed in this study for antimicrobial activity the encapsulated conjugate (PCL(PEG–Mox) NPs) did not demonstrate, conclusively, significant antibacterial activity. These systems do, however, hold promise if further developed for improved treatment of bacterial infections.

Received 24th December 2019
Accepted 16th April 2020

DOI: 10.1039/c9ra10872f

rsc.li/rsc-advances

Introduction

Since the discovery of penicillin by Sir Alexander Fleming in 1928, antibiotics have positively influenced the clinical management of bacterial infections. However, as the centenary of this first discovery approaches, major global bodies and expert groups[1,2] warn that resistance to all antibiotics is occurring at a rapid and alarming rate. According to a report published by Jim O'Neill, deaths from antimicrobial resistance could rise from the current 700 000 to 10 million per annum by 2050.[1] Further compounding the situation is that, for almost half a century there has been no new class of antibiotics discovered.[3] Aside from over-prescription, patients often do not comply with the strict regimens for treatment due to numerous drug-related toxic side effects.[4]

To improve patient compliance to treatment and ensure drug sustainability, antibiotics must be able to discriminate efficiently between the disease-causing bacteria and the healthy human host cells. Nanoparticulate drug delivery systems have shown promise for improving antimicrobial chemotherapy through reducing systemic toxicity while retaining therapeutic effect.[4] Two main options are employed for the creation of these systems – physical drug encapsulation or chemical conjugation of the drug to a polymeric carrier.[5] Encapsulation involves the physical entrapment of the drug within or adsorption onto the surface of the nanoparticle (NP) which may be made up of a hydrophobic polymer.[6] Hydrophobic polymers offer sustained drug release because they are slowly eroded in physiological

[a]*Biopolymer Modification & Therapeutics Lab, Chemicals Cluster, Council for Scientific and Industrial Research, Pretoria 0001, South Africa. E-mail: mbalogun@csir.co.za; mohammedbalogun@tuks.co.za*

[b]*Department of Chemistry, University of Pretoria, Pretoria, South Africa*

[c]*Biochemistry & Molecular Biology Department, Theodor Bilharz Research Institute, Warak El-Hadar, Kornish El-Nile, P.O. Box 30, Imbaba, 12411-Giza, Egypt*

[d]*DST/Mintek Nanotechnology Innovation Centre, Biolabels Node, Department of Biotechnology, University of the Western Cape, Cape Town, South Africa*

[e]*Infectious Disease Nanomedicine Research Group, School of Pharmacy, University of the Western Cape, Cape Town, South Africa*

† Electronic supplementary information (ESI) available. See DOI: 10.1039/c9ra10872f

fluids but drug leakage from the NP *via* diffusion or premature burst release of surface-adhered drugs during transit to the target site is often a problem.[7] Conjugation addresses this issue through covalent linkage of the drug to a carrier polymer like polyethylene glycol (PEG).[8,9] While conjugation offers this advantage, currently used carrier polymers are water-soluble.[9,10] This could result in difficulty with transmembrane transport and a rapid renal excretion of the conjugate. Batalha *et al.* recently reported on an isoniazid (INH)–polymer conjugate system for the treatment of *Mycobacterium tuberculosis* infection.[11] The delivery system involved the use of a hydrophobic polymer to which INH was linked *via* a pH-sensitive hydrazone bond and in which hydrophobic antibiotics could further be encapsulated. While this system worked well specifically against Mtb granulomas in zebra fish models it is not clear whether it could be as effective against a wider spectrum of bacteria. Also, it appears that the system is best suited for conjugation of water-soluble drugs while hydrophobic antibiotics will have to be encapsulated. This would imply that it is a best-fit model for combination drug delivery.

In an attempt to address the challenges of both encapsulation and chemical conjugation delivery systems we developed and investigated a polymer–drug conjugate (PEG–Moxifloxacin (Mox)) and an encapsulated hybrid of the conjugate where the PEG–Mox is further incorporated into a hydrophobic NP (poly(ε-caprolactone) (PCL)). PCL was chosen as it is relatively cheaper than other commonly used polyesters. Mox has been selected as a model antibiotic due to its broad-spectrum activity against both Gram negative and positive bacteria and toxic side effects which include ocular toxicity, cardiovascular toxicity (QT-interval prolongation that increases the risk of cardiac arrest), and tendon rupture.[12] It is several orders of magnitude less soluble in water than INH and more hydrophobic than rifampicin. In this work we synthesized and extensively characterized the PEG–Mox conjugate and NPs and investigated their toxicity to cells (human erythrocytes and Madin-Darby bovine kidney (MDBK) cells) and efficacy against various Gram positive and negative bacteria.

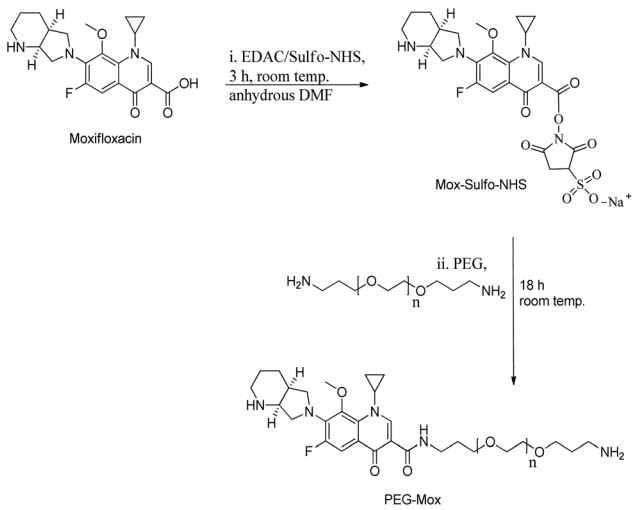

Fig. 1 Schematic of the synthesis of the PEG–Mox conjugate using carbodiimide chemistry.

Results and discussion

Synthesis and characterization of PEG–Mox conjugate and encapsulated NPs

Mox was reacted at 1.15 molar equivalents with PEG to give a stable conjugate with a zero-length amide linker (Fig. 1). Amide conjugates are resistant to rapid hydrolysis and biological degradation.[13] In using this bond in the PEG–Mox conjugate we hoped to gain insight into the performance of the entire construct in terms of mammalian and bacterial cell toxicity.

The non-ionic amphiphilic PEG–Mox conjugate, *i.e.* a hydrophilic PEG and a hydrophobic Mox, offered a polarity that

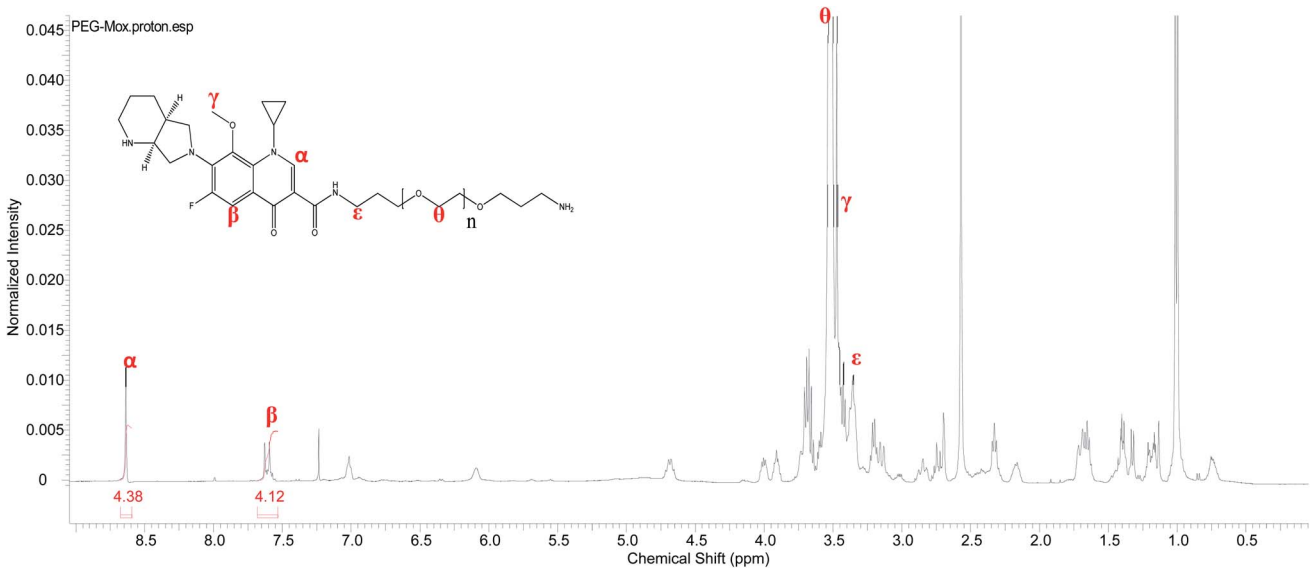

Fig. 2 Proton NMR spectrum of PEG–Mox conjugate ($CDCl_3$, 600 MHz).

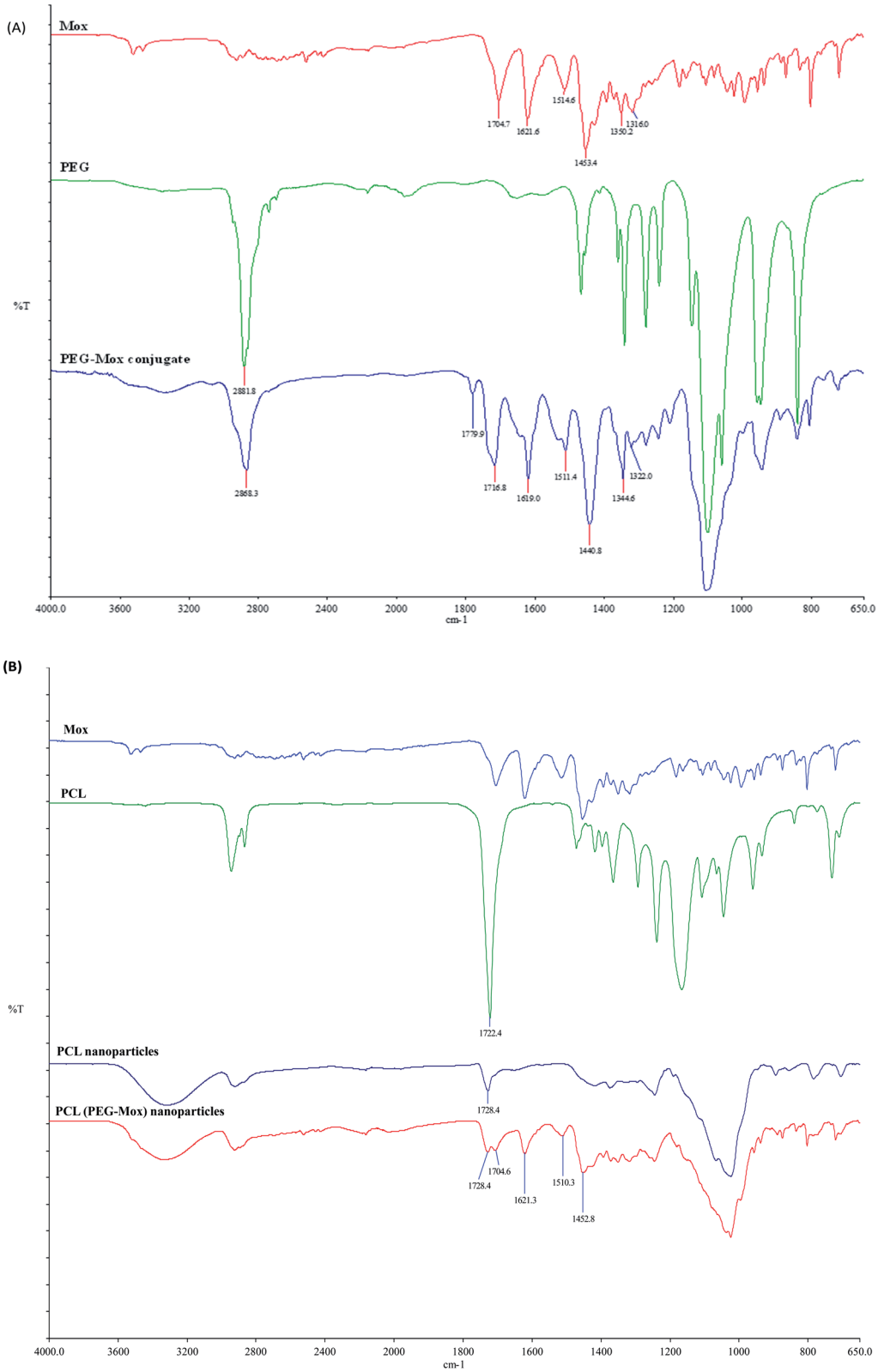

Fig. 3 FTIR spectra of (A) Mox, PEG and PEG–Mox conjugate. (B) Mox, PCL, PCL NPs, and PCL–Mox NPs.

facilitated insertion into PCL NPs. The %EE of the PEG–Mox conjugate in the PCL(PEG–Mox) NPs was determined to be 60% (w/w).

NMR and FTIR analyses

Conjugation of Mox to PEG was confirmed by ^{1}H NMR analysis. Unlike the free Mox which is insoluble in chloroform the

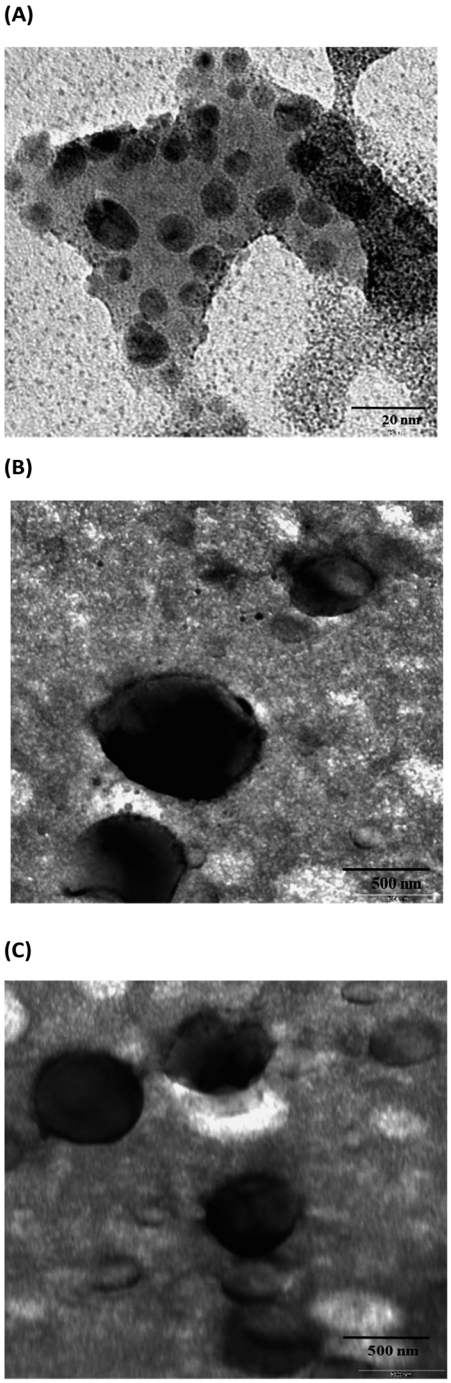

Fig. 4 TEM images: (A) PEG–Mox conjugate, (B) PCL NPs and (C) PCL(PEG–Mox) NPs.

conjugate readily dissolved in $CDCl_3$, a property conferred by the PEG. The characteristic signals of both the Mox and PEG were observed in the spectrum of the PEG–Mox conjugate (Fig. 2). The alkenyl proton (α) was the most downfield signal appearing as a singlet at 8.63 ppm while the aromatic proton (β) appeared as a doublet at 7.61 ppm. A strong singlet attributed to the three methoxy protons (γ) was observed at 3.47 ppm. Signals of PEG include the methylene protons (ε and θ) at 3.35 ppm and 3.52 ppm, respectively. The observed broadening of the signals further confirmed the successful conjugation of Mox to PEG.

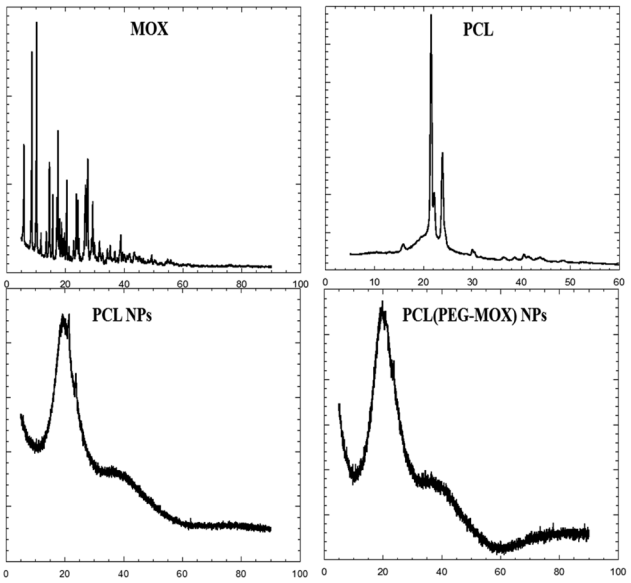

Fig. 5 X-ray diffraction patterns of Mox, molecular PCL, PCL NPs and PCL(PEG–Mox) NPs. *X*-axes represent 2 theta (degree).

Conjugation of Mox to PEG was also confirmed by ATR-FTIR with the appearance of the amide bond signal at around 1760 cm^{-1} (Fig. 3). The ATR-FTIR analysis of PCL, PCL NPs and PCL(PEG–Mox) NPs showed the characteristic peak of the PCL polymer at around 1721.4 cm^{-1} and 1725.9 cm^{-1} due to the C=O stretching vibration (Fig. 3). The spectrum of pure Mox presented functional bands at 1706 cm^{-1} due to the carboxylic acid C=O stretching vibration, C–H bonding for the substituted benzene at 1875 cm^{-1}, stretching at 1622 cm^{-1}, 1518 cm^{-1} and 1451 cm^{-1} due to aromatic C=C, and C–N banding at 1320 cm^{-1}.[14] Weak but distinctive functional bands of the Mox moiety were also found in the spectra of PCL(PEG–Mox) NPs, suggesting that most of the Mox conjugates were encapsulated into the NPs. Slight shifts in the functional bands are ascribed to amorphous packing of the PEG–Mox during the encapsulation process.

Particle morphology, size, and zeta potential

The PEG–Mox conjugate showed two average hydrodynamic diameter distributions of 8.3 ± 4 nm and 75.7 ± 10 nm in DLS studies while the PDI was observed to be 0.191. As would be expected, due to the amphiphilicity of the construct, the PEG–Mox conjugate had a spherical morphology in TEM images (Fig. 4). All the double-emulsion-prepared NPs (PCL(PEG–Mox) and empty PCL) were spherical (Fig. 5). The PCL(PEG–Mox) NPs were 241.8 ± 4 nm in diameter, significantly larger than the 174.4 ± 10 nm of empty PCL NPs. The TEM particle sizes correlated well with the DLS hydrodynamic sizes for the conjugate and the NPs. Both PCL(PEG–Mox) and empty PCL particles were of similar zeta potentials (−23.3 ± 0.9 mV and −20.3 ± 0.4 mV) and PDIs (0.24 ± 0.01 and 0.22 ± 0.02) (Table 1). These values confirmed that stable homogeneous NPs were formed. High absolute zeta potential value is an indication of stable NPs as the electrostatic repulsion prevents particle agglomeration.

Table 1 Hydrodynamic size distribution of PEG–Mox conjugate, PCL NPs and PCL(PEG–Mox) NPs obtained by DLS. N/A indicates that the particles were not charged. Data shown is the mean ± SD, $n = 3$ independent preparations

Formulation	Particle size (nm)	PDI	Zeta potential (mV)
PEG–Mox conjugate	8.3 ± 4 & 75.7 ± 10	0.19 ± 0.04	−15.2 ± 0.2
PCL NPs	174.4 ± 10	0.22 ± 0.02	−20.3 ± 0.4
PCL(PEG–Mox) NPs	241.8 ± 4	0.24 ± 0.01	−23.3 ± 0.9

XRD and TGA analyses

The physical attributes of the conjugate and NPs were also studied by XRD and TGA. The XRD patterns of the NPs (PCL NPs and PCL(PEG–Mox) NPs) presented broad signals void of any sharp peaks over the entire 2 theta (Fig. 5). This confirmed that both NPs were amorphous. On the contrary, molecular PCL showed two sharp peaks at about 21.3° and 23.9° triggered by scattering from crystalline regions. Several sharp peaks were also observed in the diffractogram of Mox. The amorphous nature of the NPs confers on them an advantage in aqueous solubility or dispersity compared to the crystalline free molecules.[15]

The PEG–Mox conjugate and PCL(PEG–Mox) NPs possessed moisture contents similar to the PEG, Mox, PCL, and PCL NPs as indicated by an initial weight loss of between 3 to 6% in TGA experiments (Fig. 6). High moisture content provides a degradative environment that could also facilitate the outward diffusion of NP content and even microbiological contamination during storage.[16] PEG rapidly decomposed between 320 to 430 °C with 89% weight loss. The PEG–Mox conjugate decomposed in a pattern more similar to the free Mox than PEG. Decomposition was initially gradual from 210 to 400 °C after the loss of water but became rapid from 400 to 435 °C. Both the empty PCL NPs and PCL(PEG–Mox) NPs showed lower thermal stability than the molecular PCL. This might be due to the NPs having a greater superficial area with thermal decomposition occurring much faster.[17]

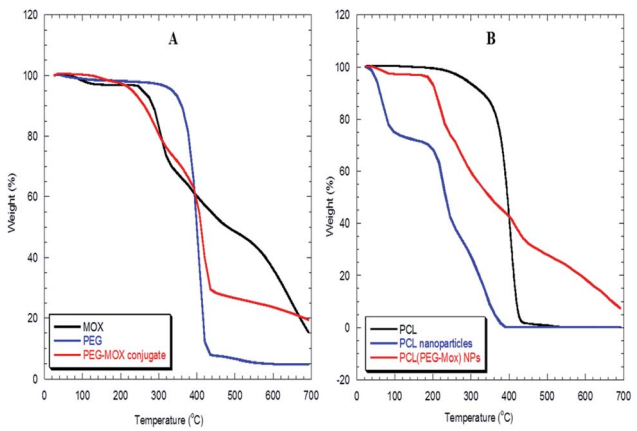

Fig. 6 TGA thermograms of (A) Mox, PEG and PEG–Mox conjugate, (B) molecular PCL, PCL NPs and PCL(PEG–Mox) NPs.

Toxicity studies

Conjugation of Mox to polysaccharides has previously been used to improve the bioavailability of the drug.[18,19] In the work of Schwartz *et al.*, Mox was conjugated to a dansylated carboxymethyl glucan which actively targeted the drug to *M. tuberculosis*-infected macrophages but the toxicity profile in human cells was not reported. It is therefore difficult to determine if the reported system offered an advantage over the free drug in terms of reduction in human toxicity.

Hemocompatibility of the formulations

To determine the effect of incorporation into a delivery vehicle on the toxicity of Mox we evaluated the biocompatibility of the conjugate and NPs in an RBC hemolysis assay (Fig. 7). At the maximum concentration of Mox tested, 1 mg mL^{-1}, the percentage hemolysis observed for free Mox, PEG–Mox and PCL(PEG–Mox) NPs were 89.0 ± 3.1, 16.2 ± 0.50 and 21.7 ± 1.5, respectively. It is clear that the delivery systems significantly attenuated the toxicity of Mox in the *ex vivo* assay and while the toxicity profile of Mox was clearly dose-dependent, that of the conjugate and the NPs were tightly restricted over the entire concentration range tested. This could translate into significant reduction in Mox systemic toxicity when used in humans.

Mox release in human plasma

Mox release from PEG–Mox conjugate and the PCL(PEG–Mox) NPs was evaluated in human plasma over 96 h. There was insignificant release of Mox from the PEG–Mox conjugate and the PCL(PEG–Mox) NPs over the 96 h period for all concentrations tested, *i.e.* 1, 3 and 5 mg mL^{-1} of the PCL(PEG–Mox) NPs (Fig. 9). This was expected as the amide linkage between the PEG and Mox is not readily labile under the physiological conditions of plasma. The hydrolysis of amides is slower than that of the esters such that amides are typically excreted in the urine unchanged.[20] Hydrolysis of amides would be expected within the intracellular acidic endolysosomal vesicles, which contain hydrolytic enzymes active at the low pH of about 5. Furthermore, PEG is capable of sterically preventing the approach of destabilizing plasma proteins to the PEG–Mox

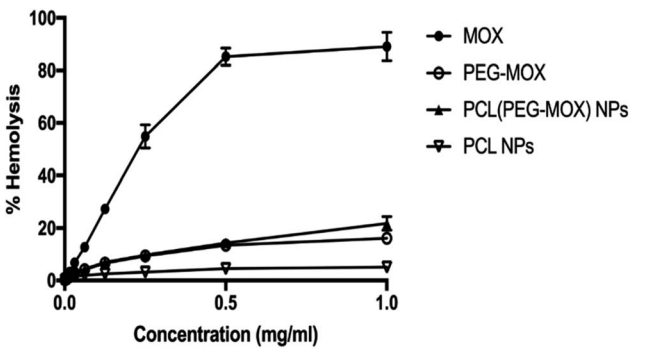

Fig. 7 *In vitro* haemolysis study with Mox, PEG–Mox conjugate, PCL(PEG–Mox) NPs and empty PCL NPs incubated with human RBC suspensions for 4 h at 37 °C. Data represents the mean ± SD, $n = 3$.

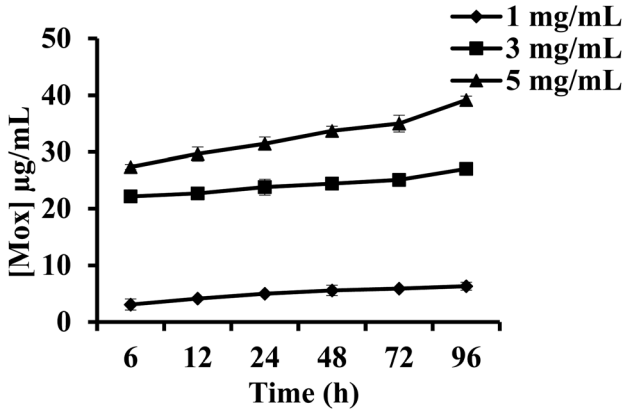

Fig. 8 *In vitro* release of Mox from PCL(PEG–Mox) NPs in human plasma over 96 h at 37 °C. Data represents the mean ± SD, $n = 3$.

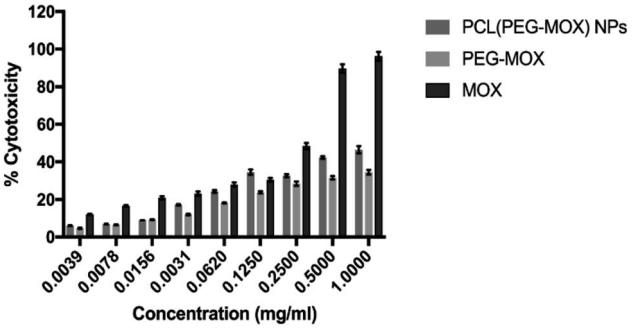

Fig. 9 Effects of Mox, PEG–Mox conjugate and PCL(PEG–Mox) NPs on MDBK cell viability measured by MTT assay. Data represent mean ± SD, $n = 3$.

conjugate or PCL(PEG–Mox) NPs.[21] As the analysis was for the free Mox molecule no significant release was detectable. This stability translates into improvement in the safety of Mox and further explains the low hemolysis observed for the two systems (Fig. 8). As the Mox is locked in macromolecular structures for both PEG–Mox and PCL(PEG–Mox), interactions with the cells are limited.[22] These results are in close agreement with previously published data.[21,23]

Cytotoxicity

The cytotoxicity of the PEG–Mox conjugate and PCL(PEG–Mox) NPs in comparison to Mox was further evaluated *in vitro* based on cellular metabolic activity using MTT assay. MDBK cell lines were used as they have defined cell junctions, polarity and a rapid growth rate.[24] In several studies MDBK cell lines have been utilized as an alternative model to Caco-2 cells.[25] PCL NPs were used as negative control and there was no discernible toxicity even at 1 mg mL^{-1}. At the highest concentration tested, *i.e.* 1.0 mg mL^{-1}, PEG–Mox conjugate and PCL(PEG–Mox) NPs induced less than 50% cell mortality, while the free Mox was more than twice as toxic at ~96.2% cell death (Fig. 9). These results correlate well with the low toxicity observed in the hemolysis assay (Fig. 7).

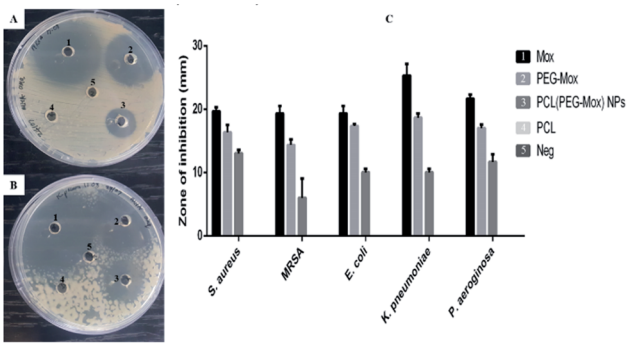

Fig. 10 Assessing the antibacterial activity of Mox, PEG–Mox, PCL(PEG–Mox) NPs and PCL NPs on Gram negative and Gram positive clinical isolates using well diffusion method. A and B are representative agar plates showing zone of inhibition for MRSA (Gram positive) and *K. pneumoniae* (Gram negative), respectively. C is a bar graph combining the data ($n = 3$) for antibacterial testing on *S. aureus*, MRSA, *E. coli, K. pneumoniae*, and *P. aeruginosa*. Empty PCL NPs did not show any activity.

In vitro microbiological assays

Antibacterial activity. The minimum inhibitory concentration (MIC) value of ≤ 32 µg mL^{-1} has been reported for Mox against various Gram-negative bacterial strains using Epsilometer test.[26] In this study, the MIC values for the free Mox and PEG–Mox on *P. aeroginosa* and *S. aureus* were observed at 25–50 µg mL^{-1} as shown in Table S1.† There was no visible growth inhibition on the other three strains, or those treated with PCL(PEG–Mox) NPs and PCL-NPs after 24 h exposure to the samples. Conjugation of Mox to PEG (PEG–Mox) appeared to elicit a moderate reduction in the drug's antibacterial activity as indicated by a diminished zone of inhibition in the well diffusion method (Fig. 10). This correlated well with the bactericidal microdilution study. The growth inhibition curves, measured as percent of viability relative to untreated cells, for PEG–Mox were very similar to the free Mox in all the microbes studied (Fig. 11). Only *E. coli* did not show any significant response to any of the test samples. Based on the viability at the lowest concentration (6.3 µg mL^{-1}) tested, *P. aeruginosa* was the most susceptible to PEG–Mox and Mox of the bacterial strains tested.

The antibacterial effects of PCL(PEG–Mox) NPs were distinctly lower when compared to free Mox and PEG–Mox although a disparity was observed between the two methods used. Interestingly in the well diffusion method the PCL(PEG–Mox) NPs showed between 10 mm to 15 mm diameter rings of inhibition which is significant in comparison to inhibition zone diameters of 15 mm to 19 mm and 20 mm to 25 mm for PEG–Mox and Mox, respectively. There was no observable effect of the empty PCL carrier (Fig. 10). On the contrary, in the microdilution experiments there was no significant difference between the PCL(PEG–Mox) NPs and the empty PCL carriers, except for *P. aeruginosa* which showed a moderate susceptibility to the former at the highest dose (100 µg mL^{-1}) tested (Fig. 11). All other strains were quite refractory to the PCL(PEG–Mox) NPs treatment. These findings demonstrate that formation of the polymer–drug conjugate retains the antibacterial activity of

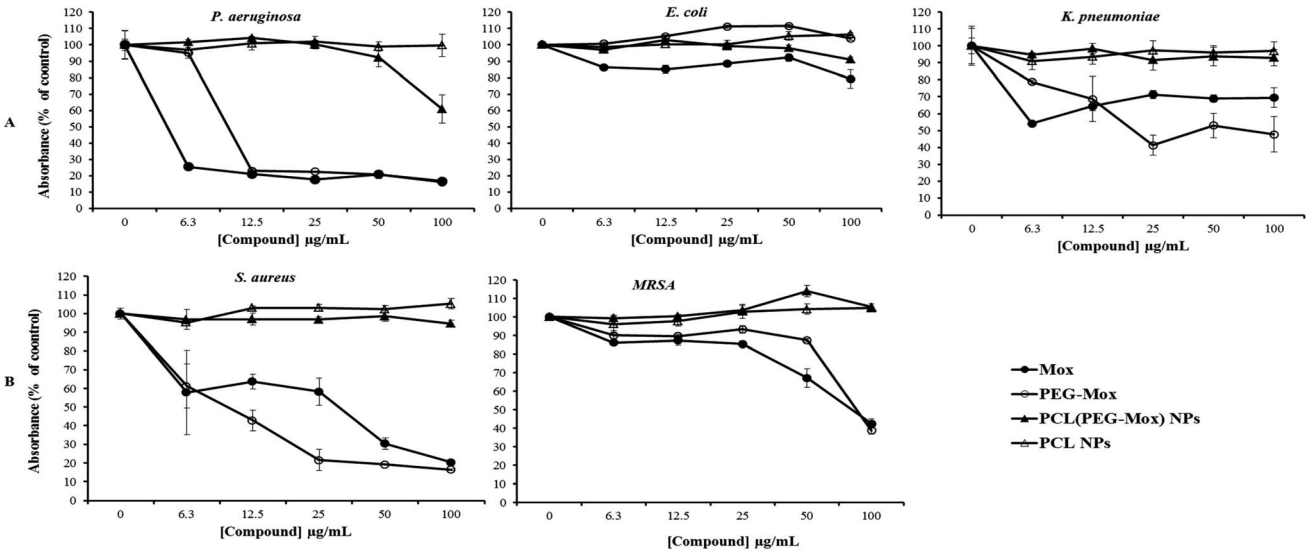

Fig. 11 Assessing the bactericidal activity of Mox, PEG–Mox, PCL(PEG–Mox) NPs and PCL NPs using the microdilution method. Gram negative (*E. coli*, *P. aeruginosa* and *K. pneumoniae*) and positive (*S. aureus*, MRSA) clinical isolates. The bacteria were exposed to the test compounds for 24 h, after which the viability of the bacteria was assessed using the AlamarBlue® assay. (A) Gram negative (*E. coli*, *P. aeruginosa* and *K. pneumoniae*) and (B) Gram positive (*S. aureus*, MRSA) clinical isolates. * indicates significant differences at $p < 0.05$.

Mox, while encapsulation of the conjugate within PCL NPs reduces the effectiveness of the conjugate. This could in part be explained by the need of the PEG–Mox conjugate to first diffuse out of the NPs or, alternatively, the PCL NP should first erode, before the activity of the PEG–Mox conjugate can be observed. A better performance might be expected *in vivo*, due to the expected action of enzymes on breaking down the NPs (and consequently releasing the conjugate). The disparities observed between the well diffusion and microdilution data could be attributed to various factors that include, but are not limited to, diffusion efficiency of the test compound, sample polarity and concentration. Due to these limitations, microdilution assays are often considered more reliable and reproducible compared to the solid agar diffusion assays.[28,29]

As the threat of losing the current arsenal of antibiotics grows, research is increasingly being focused on harnessing the potentials of drug delivery systems.[11,27,28] We have demonstrated here that the two main nanomedicine delivery systems technologies (polymer–drug conjugation and encapsulation) can be effectively utilized to reduce the toxicity of antibiotics, in this case Mox, to human cells. In *in vitro* antibacterial assays the polymer-conjugated Mox performed comparatively well with the free drug against both Gram negative and positive bacteria even while offering the possibility of an intravenous administration route due to its aqueous solubility. However, the encapsulated conjugate hybrid, PCL(PEG–Mox) NPs, did not present a definitive antibacterial performance.

Experimental

Materials

PEG ($M_w = 1.5$ KDa), PCL ($M_w = 10$ KDa), poly(vinyl alcohol) ((PVA) M_w = 13–23 KDa, 87–89% hydrolyzed), *N*-(ethylcarbonimidoyl)-*N*,*N*-dimethylpropane-1,3-diamine monohydrochloride (EDAC), *N*-hydroxysulfosuccinimide (sulfo-NHS), 2-methoxyethylmethyl (MEM), foetal bovine serum (FBS), penicillin/streptomycin, 4-(2-hydroxyethyl)-1-piperazineethanesulfonic acid (HEPES) buffer, 3-(4,5-dimethylthiazol-2-yl)-2,5-diphenyl tetrazolium bromide (MTT), 3-(4,5-dimethylthiazol-2-yl)-5-(3-carboxymethoxyphenyl)-2-(4-sulfophenyl)-2*H*-tetrazolium) (MTS), *N*,*N*-dimethylformamide (DMF), ethyl acetate, and lactose monohydrate were obtained from Sigma-Aldrich (South Africa). Mox was purchased from DB Fine Chemicals (South Africa) as the chloride salt. Madin-Darby bovine kidney (MDBK) cells stock, frozen in liquid nitrogen, ATCC no. CCL-22 passage: 46 were commercially obtained from VACSERA, Giza, Egypt. Alcohol free and drug free healthy human male donors' blood was used. All aqueous experiments were carried out in freshly prepared phosphate-buffered saline ((PBS) 137 mM NaCl; 2.7 mM KCl; 4.3 mM Na_2HPO_4; 1.47 mM KH_2PO_4 adjusted to a final pH of 7.4). Ultrapure water with resistivity of 18 MΩ cm was used in all aqueous preparations. Bacterium strains were purchased from the American Type Culture Collection (ATCC, Manassas, VA, USA).

Synthesis and characterization

Synthesis of PEG–Mox conjugate. To a stirred solution of Mox·HCl (64 mg, 0.15 mmol) in anhydrous DMF (3 mL) was added EDAC (93.12 mg, 0.6 mmol) and sulfo-NHS (116.5 mg, 0.6 mmol). The reaction was allowed to run in the dark at room temperature. After 3 h the crude solution was added dropwise to PEG (200 mg, 0.13 mmol) [dissolved in anhydrous DMF (2 mL)] and the reaction was allowed to run overnight in the dark at room temperature. At the end of the reaction period the DMF was removed under reduced pressure (7.0 mbar). Cold diethyl ether/ethanol solution (50 mL, 4 : 1 v/v) was added to the crude product and vortexed. The precipitate was collected by

centrifugation (6000 rpm, 6.0 °C), washed twice again with the same solution, dissolved in PBS buffer (pH 7.4) and finally lyophilized to obtain the PEG–Mox conjugate as yellowish powder.

Characterization of PEG–Mox conjugate. The formation of the PEG–Mox conjugate was confirmed by proton nuclear magnetic resonance (^{1}H NMR) spectroscopy and attenuated total reflectance/Fourier transform infrared (ATR/FTIR). The ^{1}H NMR experiments were run on a 600 MHz Varian INOVA or a 400 MHz Varian INOVA spectrometer. Chemical shifts (δ) are reported in parts per million (ppm) downfield with deuterated chloroform ($CDCl_3$) as solvent (referenced at 7.24 ppm). ATR/FTIR analyses were carried out between 4000 and 650 cm^{-1} using PerkinElmer Spectrum 100 FTIR spectrophotometer.

Encapsulation of PEG–Mox conjugate into PCL NPs. The synthesis of PCL *N*P-encapsulated PEG–Mox, *i.e.* PCL(PEG–Mox) NPs, was performed using a previously reported modified double-emulsion method.[29] Briefly, an aqueous solution of PVA (2% w/v, 2 mL) containing PEG–Mox conjugate (100 mg of conjugated Mox) was emulsified with a solution of PCL (100 mg) dissolved in ethyl acetate (8 mL) by homogenising with a high-speed homogeniser (Silverson L4R GX-10 model, Silverson Machines Limited, United Kingdom) rotating at 5000 rpm for 3 min. The resulting water-in-oil (w_1/o) emulsion was transferred into an aqueous solution (20 mL) of PVA (2%) and lactose (5%). The mixture was homogenised for 5 min at 8000 rpm to form a water-in-oil-in-water (w_1/o/w_2) emulsion. The emulsion was immediately spray-dried with a Buchi spray-dryer (model B-290, Buchi Labortechnik AG, Switzerland) to produce a powder of PCL(PEG–Mox) NPs. Empty PCL NPs were prepared as per the method described above, except without the addition of PEG–Mox conjugate to the formulation.

Characterization of NPs. The NPs were characterized with an ATR/FTIR as described above for the PEG–Mox conjugate. Dynamic light scattering (DLS) was measured by Malvern Zetasizer Nano ZS (Malvern, Worcestershire, UK) to determine the particle size distribution, zeta potential and polydispersity index (PDI). Typically, 1 mg of PEG–Mox conjugate, PCL or PCL(PEG–Mox) NPs was dissolved or suspended in 2 mL deionised water, filtered through a membrane syringe filter (0.2 μm) and sonicated for 10 s to ensure uniform dispersion. Transmission electron microscopy (TEM), Field Emission Electron Microscope, JEOL JEM-2100; JEOL Ltd, Japan) was also conducted to determine particle morphology. TEM samples were pre-stained with 0.5% of phosphotungstic acid and sonicated for 5 minutes.

X-ray diffraction (XRD) measurements of Mox, PCL polymer, PCL and PCL(PEG–Mox) NPs were carried out using Phillips X'Pert PRO diffractometer (PANalytical, Netherlands) under reflection–transmission mode. Samples were placed in glass sample holders and scanned from $2\theta = 5°$ to 60°, using a beam of Cu Kα radiation of $\lambda = 0.1542$ nm, operated at 45 kV, 40 mA. The scan speed and exposure time for each sample were 0.109419° s^{-1} and 17 min 27 s, respectively.

Thermogravimetric (TGA) analyses of PEG and PCL polymers, Mox, PEG–Mox conjugate, PCL and PCL(PEG–Mox) NPs were carried out using a TA Instrument (TGA Q 500, USA), using balance and sample purge nitrogen gas of 30 and 60 mL min^{-1}, respectively. Sample weights between 5.0 and 12.0 mg were used and placed into open aluminium pans. A heating rate of 10 °C min^{-1} was implemented, with a heating ramp from room temperature to 700 °C.

Encapsulation efficiency of PEG–Mox in PCL NPs. The percent encapsulation efficiency (%EE) of PEG–Mox conjugate into PCL NPs was calculated as the percentage of Mox entrapped in the PCL NPs compared with the initial amount of Mox in the conjugate. These Mox quantities were determined using a UV-vis spectrophotometer (PerkinElmer, Lambda 35, Singapore). Briefly, PCL(PEG–Mox) NPs (20 mg) were dispersed in deionised water (10 mL) and sonicated to obtain a homogeneous particle distribution. The sample was centrifuged (15 000 rpm, 10 °C) and the supernatant was analyzed at $\lambda_{max} = 290$ nm. The %EE was calculated using the equation:

$$\%\ \mathrm{EE} = \frac{\mathrm{Mox}_0 - \mathrm{Mox}_{\mathrm{supernatant}}}{\mathrm{Mox}_0} \times 100\%$$

where Mox_0 and $Mox_{supernatant}$ are the initial amount of drug in the PEG–Mox conjugate used in the production of the NPs and the amount of Mox detected in the supernatant after centrifugation of the NPs, respectively.

Toxicity assessments

Ethical clearance. Ethical approval for the use of blood from healthy human donors was obtained from the Theodor Bilharz Research Institute Institutional Review Board (TBRI-IRB) in Egypt (Reference number: FWA00010609). Informed consent was obtained from all human subjects.

Preparation of erythrocyte suspensions. Blood samples were collected from healthy human donors into BD Vacationer® Venous Blood Collection Tubes already prepared with 10–30 USP units of heparin per mL of blood to prevent clotting. 10 mL of blood was centrifuged for 10 min at 4 °C to separate plasma and erythrocytes. The retrieved erythrocytes were washed three times with six volumes of PBS (pH 7.4) buffer. The buffy coat was carefully removed with each wash. After the last wash, the packed cells were re-suspended in PBS and the hematocrit was determined.

Erythrocyte lysis (hemocompatibility) assay. Mox, PEG–Mox and PCL(PEG–Mox) NPs were dissolved or suspended in PBS and serially diluted from 1 mg mL^{-1} to 0.98 ng mL^{-1} of Mox content. PCL NPs were similarly prepared in PBS. After overnight incubation with shaking at 37 °C for all samples, 400 μL of each sample was added to 100 μL of erythrocyte suspension (1 mL of packed cells in 10 mL PBS). PBS solution and 1% w/v solution of Triton X100 were used for negative and positive controls, respectively. After 4 h of incubation at 37 °C, the samples were centrifuged for 10 min at 2000 rpm, the supernatant was withdrawn and hemolysis was determined from the 540 nm absorbance of hemoglobin released into the supernatant using a UV-vis spectrophotometer (Abbotta Kinetic Spectrophotometer, New Jersey, USA). The results are expressed as percent hemolysis and were calculated according to the equation:

$$\%\ \text{hemolysis} = \frac{\text{Ave.Abs}_{\text{sample}} - \text{Ave.Abs}_{\text{neg}}}{\text{Abs}_{\text{max.pos}}} \times 100\%$$

where $\text{Ave.Abs}_{\text{sample}}$ is the average absorbance of the sample, $\text{Ave.Abs}_{\text{neg}}$ is the average absorbance of the negative control and $\text{Abs}_{\text{max.pos}}$ is the maximum absorbance of the positive control.

Toxicity against MDBK cell line. Madin-Darby bovine kidney (MDBK) cells were grown in MEM growth medium supplemented with 10% fetal bovine serum, 1% penicillin/streptomycin and 1% HEPES buffer. The cells were seeded in a 96-well culture plate at a density of 4×10^4 cells per mL and incubated for 24 h at 37 °C to reach 70% confluency. Cells were treated with 0–1 mg mL^{-1} of each test substance (Mox, PEG–Mox conjugate, PCL(PEG–Mox) NPs) and PCL NPs for 48 h. The formulation stock solutions were dissolved or suspended in PBS (pH 7.4), serial dilution of each formulation was prepared using MEM. After 48 h, the medium was replaced with 200 μL of fresh medium. MTT dye (50 μL, 5 mg mL^{-1}) was added to each well and further incubated for 4 h. The liquid medium containing MTT was removed and DMSO (200 μL) was added to solubilize the formazan crystals. The absorbance was measured at $\lambda_{max} =$ 490 nm using an ELX-50 plate reader (Bioteck Instrument, USA) using reference wavelength of 655 nm. The percent cytotoxicity was calculated according to the equation:

$$\%\ \ \text{cytotoxicity} = \left[\frac{\text{Abs}_{\text{sample}} - \text{Abs}_{\text{blank}}}{\text{Abs}_{\text{mc}} - \text{Abs}_{\text{blank}}}\right] \times 100\%$$

where $\text{Abs}_{\text{sample}}$ is the absorbance of the sample, $\text{Abs}_{\text{blank}}$ is the absorbance of the blank and Abs_{mc} is the absorbance of the control medium.

Release of Mox from PCL(PEG–Mox) NPs in human plasma. The stability of the PCL(PEG–Mox) NPs, *i.e.* the release of Mox from the PCL(PEG–Mox) NPs, was studied *in vitro* in human plasma. Fresh whole blood samples were obtained from healthy human donors at TBRI and stored in EDTA tubes to inhibit blood clotting. The blood samples were centrifuged for 10 min to pellet the erythrocytes and collect the plasma. The PCL(PEG–Mox) NPs were suspended in PBS (pH 7.4) to three different concentrations with respect to the Mox content, *i.e.* 1.0 mg mL^{-1}, 3.0 mg mL^{-1} and 5.0 mg mL^{-1}. The experiment was initiated with the addition of 400 μL of the PCL(PEG–Mox) NPs suspensions to 1 mL of plasma and incubated at 37 °C with gentle shaking. At regular time intervals (6, 12, 24, 48, 72, and 96 h), 100 μL of plasma solution was drawn and immediately placed on ice to retard any further reactions. The same procedure was carried out to investigate the release of Mox from the PEG–Mox conjugate but this was done only at 1 mg mL^{-1}. HPLC-grade acetonitrile (135 μL) was added to precipitate the plasma proteins which were pelleted by centrifugation at 14 000 rpm for 5 min. The supernatant was withdrawn and analysed by HPLC (LC-10A, Shimadzu Kyoto, Japan) equipped with a SunFire column C18 (5 μm × 250 mm) and a SunFire Guard column C18 (5 μm × 20 mm) to quantify Mox. The mobile phase (acetonitrile 30%, methanol 30%, phosphate buffer 40%), was injected at a flow rate of 1 mL min^{-1} and elution under isocratic conditions. The λ_{max} for detecting Mox was 290 nm. The procedure above was also applied to plasma alone to determine its corresponding chromatogram to correct for matrix interference.

Antimicrobial activity assessment

Two Gram-positive bacterial (*Staphylococcus aureus* (*S. aureus*, ATCC no. 25923) and methicillin-resistant *S. aureus* (MRSA, ATCC no. 33591) and three Gram-negative bacterial (*Escherichia coli* (*E. coli*, ATCC no. 35218), *Pseudomonas aeruginosa* (*P. aeruginosa*, ATCC no. 27853) and *Klebsiella pneumoniae* (*K. pneumoniae*, ATCC no. 13883) were studied in this work and the bacteria were handled and tested according to the guidelines set by the Clinical and Laboratory Standard Institute (CLSI, 2015). The glycerol stocks containing the selected bacteria were streaked on agar plates (31 g L^{-1} Nutrient agar, Merck, South Africa) and cultured for 24 h. Colonies were selected from agar plates and cultured in nutrient broth (16 g L^{-1} Nutrient broth, Merck, South Africa) for further tests.

The antibacterial activities of the Mox, PEG–Mox conjugate, PCL(PEG–Mox) NPs and PCL NPs were evaluated against the selected bacteria using an agar well diffusion method. The organisms were sub-cultured in nutrient broth at 37 °C for 18 to 24 h. The cultures were diluted in nutrient broth to 1×10^8 CFU mL^{-1} (equivalent to 0.5 Mcfarland). The diluted cultures were swabbed onto nutrient agar plates. The test samples (10 μL from a 100 μg mL^{-1} stock solution) were added to the wells and the plates were incubated at 37 °C for 24 h. The experiments were performed in triplicates. After 24 h, the diameters of the inhibition zones around the wells were measured in millimeters.

The bactericidal effects of the test samples were also evaluated by the microdilution method using the AlamarBlue® assay.[30] The active ingredient of the AlamarBlue® reagent (Invitrogen, USA), resazurin is converted to resorufin by viable cells and can be quantified by measuring the absorbance of the test sample at $\lambda_{max} = 570$ nm. Absorbance is therefore directly proportional to the number of viable cells. Bacterial suspensions containing 1×10^8 CFU mL^{-1} were prepared for all the bacterial strains. These bacterial suspensions were transferred into 96-well plates, 100 μL per well. The test samples were added to the bacterial cultures and the plates were incubated at 37 °C for 24 h. The concentrations of the test samples ranged from 0 μg mL^{-1} to 100 μg mL^{-1}. After 24 h treatment, the lowest concentration of the samples that inhibited visible growth of the bacteria was recorded as the MICs. Thereafter, AlamarBlue® reagent was added (10 μL per well) to each well. The plate was incubated in the dark for 3 h at 37 °C. Absorbance of each well was read at $\lambda_{max} = 570$ and 700 nm using a POLARstar® Omega (BMG Labtech, Germany) and expressed as percentage viability (percentage of absorbance of untreated control) of the growth control.

Statistical analysis

All experiments were performed at least in triplicates and the results are expressed as mean ± standard deviation (S.D.). Data were analysed by the Student's *t*-test using GraphPad Prism version 8.0.0 for MacOS (GraphPad Software, La Jolla California USA). Statistical differences were considered at $p < 0.05$.

Conclusions

This work described the synthesis of a PEG–Mox conjugate which is further encapsulated within a polymeric NP, forming a novel hybrid delivery system of the drug. These designs offer more versatility for delivery of the Mox to treat antimicrobial infections, *e.g. via* intravenous or inhalation routes in addition to the current oral route. Our work has shown that the toxicity of Mox to human erythrocytes and MDBK cells can be effectively attenuated while retaining significant antibacterial activity by incorporation into a polymeric delivery system. Chemical conjugation of the drug to a polymeric carrier ensured that free Mox would not be released in extracellular fluids like plasma. The system described in this work holds promise for the development of effective treatments of bacterial infections which are more tolerable by patients.

Conflicts of interest

There are no conflicts to declare.

Acknowledgements

This work is based on a bilateral research project supported in part by the National Research Foundation of South Africa (Grant Number: 82819, 114369) and the Ministry of Higher Education and Scientific Research, Egypt (Project No. 17-2-120).

References

1 J. O'Neill, *Tackling Drug-resistant Infections Globally: Final Report and Recommendations–The Review on Antimicrobial Resistance Chaired by Jim O'Neill*, Wellcome Trust and HM Government, London, 2016.
2 U. Hofer, The cost of antimicrobial resistance, *Nat. Rev. Microbiol.*, 2019, **17**(1), 3.
3 E. Tacconelli, N. Magrini, G. Kahlmeter and N. Singh, *Global priority list of antibiotic-resistant bacteria to guide research, discovery, and development of new antibiotics*, World Health Organization, 2017, vol. 27.
4 P. N. Prasad, *Introduction to nanomedicine and nanobioengineering*, John Wiley & Sons, 2012.
5 R. K. Tekade, R. Maheshwari, N. Soni, M. Tekade and M. B. Chougule, Chapter 1 - Nanotechnology for the Development of Nanomedicine, in *Nanotechnology-Based Approaches for Targeting and Delivery of Drugs and Genes*, ed. V. Mishra, P. Kesharwani, M. C. I. Mohd Amin and A. Iyer, Academic Press, 2017, pp. 3–61.
6 C. Wischke and S. P. Schwendeman, Principles of encapsulating hydrophobic drugs in PLA/PLGA microparticles, *Int. J. Pharm.*, 2008, **364**(2), 298–327.
7 J. M. Barichello, M. Morishita, K. Takayama and T. Nagai, Encapsulation of Hydrophilic and Lipophilic Drugs in PLGA Nanoparticles by the Nanoprecipitation Method, *Drug Dev. Ind. Pharm.*, 1999, **25**(4), 471–476.
8 I. Ekladious, Y. L. Colson and M. W. Grinstaff, Polymer–drug conjugate therapeutics: advances, insights and prospects, *Nat. Rev. Drug Discovery*, 2019, **18**(4), 273–294.
9 S. Mvango, W. M. R. Matshe, A. O. Balogun, L. A. Pilcher and M. O. Balogun, Nanomedicines for Malaria Chemotherapy: Encapsulation vs. Polymer Therapeutics, *Pharm. Res.*, 2018, **35**(12), 237.
10 A. Duro-Castano, M. Talelli, G. Rodríguez-Escalona and M. J. Vicent, Chapter 13 - Smart Polymeric Nanocarriers for Drug Delivery, in *Smart Polymers and their Applications*, ed. M. R. Aguilar and J. San Román, Woodhead Publishing, 2nd edn, 2019, pp. 439–479.
11 I. L. Batalha, A. Bernut, M. Schiebler, M. M. Ouberai, C. Passemar, C. Klapholz, *et al.*, Polymeric nanobiotics as a novel treatment for mycobacterial infections, *J. Controlled Release*, 2019, **314**, 116–124.
12 T. (Edinb), Moxifloxacin, *Tuberculosis*, 2008, **88**(2), 127–131.
13 R. J. Ouellette and J. D. Rawn, 12 - Amines and Amides, in *Principles of Organic Chemistry*, ed. R. J. Ouellette and J. D. Rawn, Elsevier, Boston, 2015, pp. 315–342.
14 A. Mahor, S. K. Prajapati, A. Verma, R. Gupta, A. K. Iyer and P. Kesharwani, Moxifloxacin loaded gelatin nanoparticles for ocular delivery: formulation and *in vitro*, *in vivo* evaluation, *J. Colloid Interface Sci.*, 2016, **483**, 132–138.
15 S. B. Murdande, M. J. Pikal, R. M. Shanker and R. H. Bogner, Aqueous solubility of crystalline and amorphous drugs: Challenges in measurement, *Pharm. Dev. Technol.*, 2011, **16**(3), 187–200.
16 C. Vauthier and K. Bouchemal, Methods for the Preparation and Manufacture of Polymeric Nanoparticles, *Pharm. Res.*, 2009, **26**(5), 1025–1058.
17 R. M. Mainardes, M. P. D. Gremião and R. C. Evangelista, Thermoanalytical study of praziquantel-loaded PLGA nanoparticles, *Rev. Bras. Cienc. Farm.*, 2006, **42**, 523–530.
18 Y. S. Schwartz, M. I. Dushkin, V. A. Vavilin, E. V. Melnikova, O. M. Khoschenko, V. A. Kozlov, *et al.*, Novel conjugate of moxifloxacin and carboxymethylated glucan with enhanced activity against Mycobacterium tuberculosis, *Antimicrob. Agents Chemother.*, 2006, **50**(6), 1982–1988.
19 N. S. Abbas, M. Amin, M. A. Hussain, K. J. Edgar, M. N. Tahir and W. Tremel, Extended release and enhanced bioavailability of moxifloxacin conjugated with hydrophilic cellulose ethers, *Carbohydr. Polym.*, 2016, **136**, 1297–1306.
20 D. A. Hartman, Determination of the Stability of Drugs in Plasma, *Curr. Protoc. Pharmacol.*, 2002, **19**(1), 7.6.1–7.6.8.
21 H. Heiati, R. Tawashi and N. C. Phillips, Solid lipid nanoparticles as drug carriers: II. Plasma stability and biodistribution of solid lipid nanoparticles containing the lipophilic prodrug 3′-azido-3′-deoxythymidine palmitate in mice, *Int. J. Pharm.*, 1998, **174**(1), 71–80.
22 R. Duncan, P. Ferruti, D. Sgouras, A. Tuboku-Metzger, E. Ranucci and F. Bignotti, A Polymer-Triton X-100 Conjugate Capable of PH-Dependent Red Blood Cell Lysis: A Model System Illustrating the Possibility of Drug Delivery Within Acidic Intracellular Compartments, *J. Drug Targeting*, 1994, **2**(4), 341–347.

23 K. Letchford, R. Liggins, K. M. Wasan and H. Burt, In vitro human plasma distribution of nanoparticulate paclitaxel is dependent on the physicochemical properties of poly(ethylene glycol)-block-poly(caprolactone) nanoparticles, *Eur. J. Pharm. Biopharm.*, 2009, **71**(2), 196–206.

24 M. Trif, P. E. Florian, A. Roseanu, M. Moisei, O. Craciunescu, C. E. Astete, *et al.*, Cytotoxicity and intracellular fate of PLGA and chitosan-coated PLGA nanoparticles in Madin–Darby bovine kidney (MDBK) and human colorectal adenocarcinoma (Colo 205) cells, *J. Biomed. Mater. Res., Part A*, 2015, **103**(11), 3599–3611.

25 Y. Lai, P.-C. Chiang, J. D. Blom, N. Li, K. Shevlin, T. G. Brayman, *et al.*, Comparison of In vitro Nanoparticles Uptake in Various Cell Lines and In vivo Pulmonary Cellular Transport in Intratracheally Dosed Rat Model, *Nanoscale Res. Lett.*, 2008, **3**(9), 321.

26 A. Grillon, F. Schramm, M. Kleinberg and F. Jehl, Comparative Activity of Ciprofloxacin, Levofloxacin and Moxifloxacin against Klebsiella pneumoniae, Pseudomonas aeruginosa and Stenotrophomonas maltophilia Assessed by Minimum Inhibitory Concentrations and Time-Kill Studies, *PLoS One*, 2016, **11**(6), e0156690.

27 S. Alven, B. A. Aderibigbe, M. O. Balogun, W. M. R. Matshe and S. S. Ray, Polymer-drug conjugates containing antimalarial drugs and antibiotics, *J. Drug Delivery Sci. Technol.*, 2019, **53**, 101171.

28 A. J. Huh and Y. J. Kwon, "Nanoantibiotics": a new paradigm for treating infectious diseases using nanomaterials in the antibiotics resistant era, *J. Controlled Release*, 2011, **156**(2), 128–145.

29 L. Tshweu, L. Katata, L. Kalombo and H. Swai, Nanoencapsulation of water-soluble drug, lamivudine, using a double emulsion spray-drying technique for improving HIV treatment, *J. Nanopart. Res.*, 2013, **15**(11), 2040.

30 G.-X. Wei, A. N. Campagna and L. A. Bobek, Effect of MUC7 peptides on the growth of bacteria and on Streptococcus mutans biofilm, *J. Antimicrob. Chemother.*, 2006, **57**(6), 1100–1109.